Materials Advances

ROYAL SOCIETY OF CHEMISTRY

PAPER

View Article Online
View Journal | View Issue

Check for updates

Cite this: *Mater. Adv.*, 2026, 7, 2499

Mitochondria targeted small molecule-mediated chemo-photodynamic therapy induces apoptosis in cancer cells

Tripti Mishra, Phanindra Kumar, Sanyam, Asima Sahu, Anirban Mondal and Sudipta Basu *

Mitochondria, the powerhouse of the cell, play a vital role in bioenergetics, biosynthesis, and stress signaling, making them a promising target for anti-cancer therapy. However, achieving precise mitochondrial targeting remains challenging. Recently, phototherapy has gained attention for its non-invasive nature, yet the development of mitochondria-targeted small molecule probes for phototherapy is still limited. To address this, we design and synthesize Cy-$(Indo)_2$, a mitochondria-targeted small molecule featuring a pentamethine cyanine-based donor–π–acceptor system for simultaneous fluorescence imaging and phototherapy along with Cox-2 inhibition *via* conjugation with indomethacin V. Cy-$(Indo)_2$ self-assembles into nanoscale particles in water with a high positive surface charge, localizes in the mitochondria of HCT-116 colon cancer cells within 3 h, and generates ROS within 20 min under 740 nm LED irradiation. Molecular dynamics (MD) simulations and time-dependent density functional theory (TD-DFT) confirmed the self-assembly of Cy-$(Indo)_2$ into nanoparticles as well as effective spin–orbit coupling in the excited states to stabilize the T_1 state for efficient photodynamic therapy (PDT). Under 740 nm LED light (0.9 W cm^{-2}), Cy-$(Indo)_2$ induces mitochondrial outer membrane permeabilization (MOMP), triggering mitochondrial impairment, ROS generation, and apoptosis *via* Bcl-2, Cas-3, Cas-9, PARP and Cox-2 inhibition as well as BAX upregulation. This mitochondria-targeted chemo-photodynamic effect results in selective HCT-116 death without showing toxicity to non-cancerous Cos-7 cells. Our findings establish Cy-$(Indo)_2$ as a promising organelle-specific therapeutic, opening new avenues for light-based, non-invasive cancer treatment.

Received 5th August 2025,
Accepted 11th January 2026

DOI: 10.1039/d5ma00853k

rsc.li/materials-advances

Open Access Article. Published on 13 January 2026. Downloaded on 4/16/2026 7:27:41 PM.
This article is licensed under a Creative Commons Attribution-NonCommercial 3.0 Unported Licence.

Introduction

Mitochondria, often referred to as the powerhouse of the cell, are among the most critical sub-cellular organelles, orchestrating a myriad of biological processes, including ATP synthesis, metabolism, bioenergetics, and cell death signaling.[1–5] Dysregulation of these pathways can lead to mitochondrial malfunction, which in turn is implicated in various pathological conditions, including cancer.[6–9] Consequently, the development of novel small molecules targeting mitochondria in cancer cells has emerged as a promising alternative therapeutic strategy.[10–20] However, conventional small-molecule chemotherapeutic drugs often cause collateral damage to non-cancerous cells and tissues, leading to undesirable side effects.

In this context, photodynamic therapy (PDT), which leverages biocompatible light to activate small-molecule photosensitizers, has gained significant attention as a non-invasive approach to cancer treatment. This process generates reactive oxygen species (ROS), which induce cancer cell death.[21–24] Despite the challenges associated with their design, synthesis, and purification, porphyrins and phthalocyanines have long dominated the field of PDT as photosensitizers.[25–30] More recently, cyanine dyes have been extensively explored for phototherapy due to their excellent optical properties.[31–34] However, the development of mitochondria-targeted small molecules capable of integrating both chemo- and photodynamic therapy remains largely unexplored.[35–41]

To address this, we have designed and synthesized a novel small molecule, Cy-$(Indo)_2$ (Fig. 1a), through a concise strategy by incorporating a cationic pentamethine cyanine moiety for (a) mitochondria-specific homing, (b) sub-cellular fluorescence imaging, and (c) photodynamic therapy, along with indomethacin V (Fig. 1b), a non-steroidal anti-inflammatory drug (NSAID) for inhibiting mitochondrial cyclooxygenase-2 (Cox-2). Remarkably, Cy-$(Indo)_2$ self-assembled into spherical nanoparticles in water, which was confirmed by molecular dynamics (MD) simulations, exhibiting a high positive surface charge and

Department of Chemistry, Indian Institute of Technology (IIT) Gandhinagar, Palaj, Gandhinagar, Gujarat, 382355, India. E-mail: Sudipta.basu@iitgn.ac.in

© 2026 The Author(s). Published by the Royal Society of Chemistry

Open Access Article. Published on 13 January 2026. Downloaded on 4/16/2026 7:27:41 PM. This article is licensed under a Creative Commons Attribution-NonCommercial 3.0 Unported Licence.

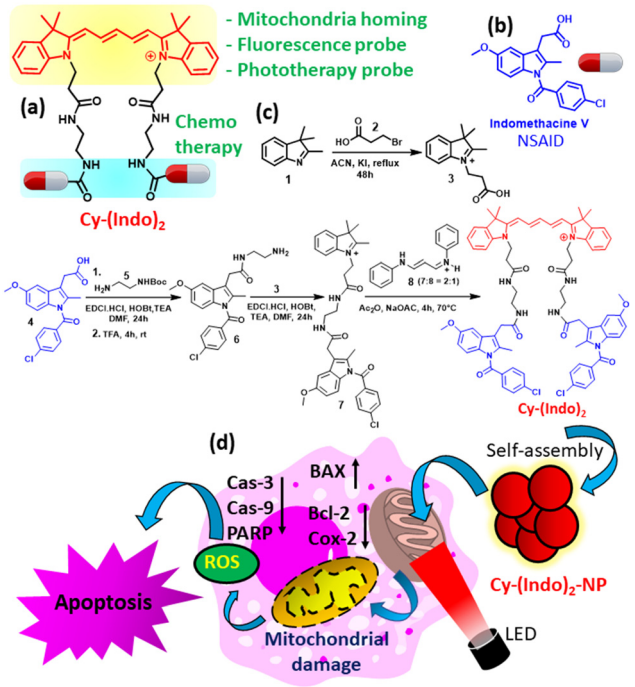

Fig. 1 (a) Chemical structure of Cy-(Indo)$_2$, (b) chemical structure of indomethacin V, (c) synthetic scheme of Cy-(Indo)$_2$, and (d) schematic representation of self-assembly of Cy-(Indo)$_2$ into nanoparticles and the mechanism of mitochondria targeted chemo-photodynamic therapy in cancer cells towards apoptosis.

generating ROS upon irradiation with white light and a 740 nm LED for photodynamic therapy. Interestingly, time-dependent density functional theory (TD-DFT) exhibited effective spin–orbit coupling between S_1 and T_1 states leading to the stabilization and extended lifetime of the T_1 state for efficient PDT. Furthermore, Cy-(Indo)$_2$ successfully localized within the mitochondria of HCT-116 colon cancer cells within 3 h. Upon exposure to 740 nm LED light, it induced mitochondrial outer membrane permeabilization (MOMP) and structural damage, leading to the production of intracellular ROS and superoxide species (Fig. 1d). This mitochondrial impairment subsequently triggered apoptosis by inhibiting Cox-2 and the anti-apoptotic proteins Bcl-2, Cas-3, Cas-9 and PARP, and upregulating pro-apoptotic BAX, resulting in significant colon cancer cell death, while exhibiting no toxicity toward non-cancerous Cos-7 kidney fibroblast cells. This novel small-molecule-mediated chemo-photodynamic approach to mitochondrial impairment paves the way for a deeper understanding of the chemical biology of light–matter interactions within specific organelles, offering a promising direction for future non-invasive cancer therapies.

Result and discussion

We hypothesized to design a mitochondria targeted small molecule [Cy-(Indo)$_2$] consisting of (a) a cationic pentamethine cyanine-based donor–π–acceptor moiety for simultaneous mitochondria homing, fluorescence imaging and phototherapy under NIR light irradiation and (b) indomethacin V (Fig. 1b), a non-steroidal anti-inflammatory drug (NSAID) for spatial inhibition of cyclooxygenase-2 (Cox-2) in mitochondria (Fig. 1a). Moreover, the photophysical properties of pentamethine cyanine can be further tuned towards the NIR-II region for deep tissue penetration for theranostic applications. To synthesize Cy-(Indo)$_2$, we first reacted 2,3,3-trimethylindolenine (**1**) with 3-bromopropionic acid (**2**) in the presence of potassium iodide in refluxing conditions to obtain 1-(2-carboxyethyl)-2,3,3-trimethyl-3*H*-indol-1-ium (**3**) (Fig. 1c). On the other hand, we reacted indomethacin V (**4**) with mono-Boc-protected ethylenediamine (**5**) using EDCI·HCl and HOBt as coupling agents followed by deprotection of the Boc-group to obtain an indomethacin V–ethylenediamine conjugate (**6**). Furthermore, compound **6** was reacted with compound **3** using EDCI·HCl and HOBt as coupling agents to obtain the conjugated product **7**, which was finally reacted with compound **8** in a 2 : 1 molar ratio in the presence of acetic anhydride and sodium acetate to afford Cy-(Indo)$_2$. All the intermediates and the final compound were characterized by ^{1}H and ^{13}C NMR, and HR-MS spectroscopy (Fig. S1–S12). We also evaluated the UV-vis and fluorescence spectroscopy of Cy-(Indo)$_2$, which showed that Cy-(Indo)$_2$ absorbed at 650.5 nm and emitted at 676 nm (Fig. S13), suitable for phototherapy as well as sub-cellular fluorescence imaging.

Due to the amphiphilic nature, we anticipated that Cy-(Indo)$_2$ would self-assemble in water. We evaluated the self-assembly of Cy-(Indo)$_2$ in water and measured the hydrodynamic diameter and surface charge by dynamic light scattering (DLS). The hydrodynamic diameter was found to be 284 nm (Fig. 2a) with a zeta potential of +41.5 mV, highly favourable for accumulation into the mitochondria due to its high negative potential. We checked the size of Cy-(Indo)$_2$ in DMEM cell culture media having 10% fetal bovine serum (FBS), which showed a hydrodynamic diameter = 310 nm (Fig. S14a) confirming the self-assembly in the cellular microenvironment also. To assess the concentration dependence of the self-assembly, we measured the scattering intensity of light of Cy-(Indo)$_2$ in water in a concentration dependent manner through DLS. We observed a sharp increase in the scattering intensity at 100 nM concentration, which indicated that Cy-(Indo)$_2$ self-assembled into nanoparticles at 100 nM concentration (Fig. S14b).

We further visualized the size, shape and morphology of the self-assembled Cy-(Indo)$_2$ by scanning electron microscopy (SEM) and atomic force microscopy (AFM). Both the SEM and AFM images confirmed that Cy-(Indo)$_2$ self-assembled into spherical nanoscale particles [Cy-(Indo)$_2$-NPs] in water (Fig. 2b and c and Fig. S15). We also confirmed the self-assembly of Cy-(Indo)$_2$ in water by the Tyndall effect (Fig. S16).

We further checked the stability of the Cy-(Indo)$_2$-NPs at 4 °C as well as under physiological conditions at 37 °C by measuring the size and the zeta potential in a time-dependent manner. We observed that at 4 °C, the size of the Cy-(Indo)$_2$-NPs decreased from 284.1 nm to 169 nm over 4 days and increased to 420 nm on the 5th day (Fig. S17a). On the other hand, at 37 °C, the size of the Cy-(Indo)$_2$-NPs gradually increased until 488 nm over 5 days. Interestingly, the zeta potential of the Cy-(Indo)$_2$-NPs

© 2026 The Author(s). Published by the Royal Society of Chemistry

Open Access Article. Published on 13 January 2026. Downloaded on 4/16/2026 7:27:41 PM.
This article is licensed under a Creative Commons Attribution-NonCommercial 3.0 Unported Licence.

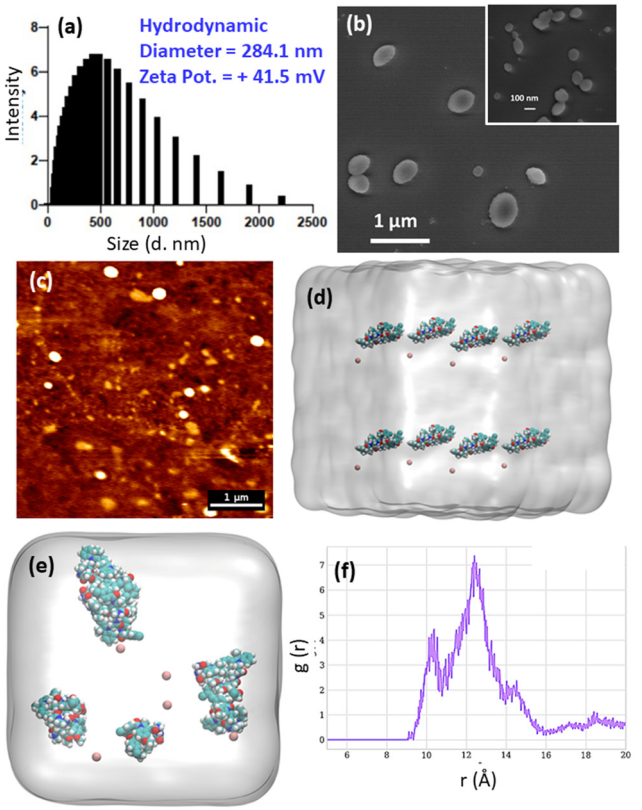

Fig. 2 (a) Hydrodynamic diameter and zeta potential of the self-assembled nanoparticles of Cy-(Indo)$_2$ in water measured by dynamic light scattering (DLS). (b) and (c) SEM and AFM images of the self-assembled nanoparticles of Cy-(Indo)$_2$ in water. (d) Initial configuration of the molecule before the simulation. (e) Final configuration after the equilibration step, showing the formation of dimer and trimer aggregates. (f) Radial distribution function (RDF) of Cy-(Indo)$_2$, showing the distance between the centers of mass (COM) of the molecules.

decreased gradually from +41.5 mV to +7 mV and +12.3 mV at 4 °C and 37 °C, respectively, over 5 days (Fig. S17b). These time-dependent size and zeta potential measurements indicated that the Cy-(Indo)$_2$-NPs remained stable under physiological conditions for 3–4 days.

The MD simulations offered valuable insights into the self-assembly behavior of Cy-(Indo)$_2$ in an aqueous environment. To eliminate any bias toward aggregation at the outset, the molecules were initially placed at sufficiently large separations, ensuring no close contacts in the starting configuration. As illustrated in Fig. 2d, the initial arrangement confirms the absence of any pre-formed aggregates. Over the course of the simulation, the molecules exhibited a clear tendency to self-associate, ultimately forming stable dimer and trimer aggregates. The final configuration, shown in Fig. 2e, highlights this spontaneous aggregation behavior, supporting the proposed self-assembly mechanism. To further quantify the extent of molecular association, a radial distribution function (RDF) analysis was performed, calculating the distribution of distances between the centers of mass (COM) of the Cy-(Indo)$_2$ molecules. As shown in Fig. 2f, the RDF reveals distinct peaks at approximately 10.5 Å and 13.0 Å, corresponding to preferred intermolecular separations in the aggregated state. These features reflect characteristic distances between molecules within dimers and higher-order aggregates, confirming the formation of stable self-assembled structures during the simulation. These DLS, SEM, AFM and MD simulations confirmed that Cy-(Indo)$_2$ indeed self-assembled into nano-scale particles, which can efficiently home into the tumor tissues by the enhanced permeability and retention (EPR) effect in the animal models to increase the anti-cancer efficacy with less toxic side effects in the healthy tissues.[42]

For successful phototherapy, the molecule should show absorbance at the same wavelength as the irradiated light. Despite having absorbance at 650 nm, we could not use the light in that range due to their lack of biocompatibility leading to cytotoxicity to the cells.[43–47] Moreover, we recently showed that 740 nm LED (0.9 W cm^{-2}) light is biocompatible.[48] Furthermore, following ground-state geometry optimization, the absorption properties of Cy-(Indo)$_2$ were investigated using TD-DFT calculations. The computed absorption spectrum, shown in Fig. 3a, revealed a broad absorption profile extending from 400 to 800 nm, with an intense peak centered around 500 nm. Notably, although the absorption intensity in the vicinity of 740 nm is relatively weak, TD-DFT predicts the presence of an electronic transition at this wavelength, suggesting a non-negligible probability of light absorption despite its low magnitude. An analysis of the frontier molecular orbitals was also performed to elucidate the nature of the observed transitions further. The highest occupied molecular orbital (HOMO) is characterized by non-bonding electron density, whereas the lowest unoccupied molecular orbital (LUMO) exhibits typical π*-antibonding character (Fig. 3b). The electronic transition responsible for the absorption near 740 nm primarily involves an n → π* excitation, which is supported

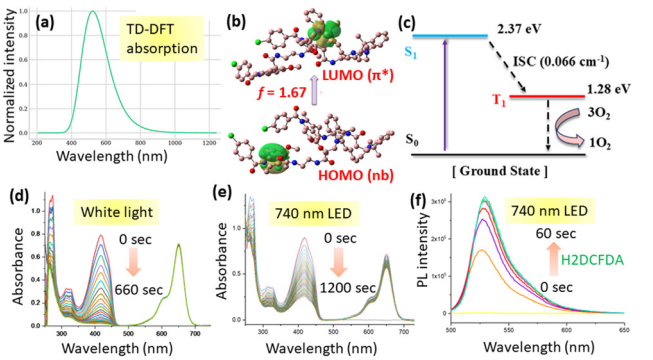

Fig. 3 (a) Absorption spectrum of Cy-(Indo)$_2$ obtained *via* TD-DFT calculations at the B3LYP/Def2-SVP level of theory. (b) Frontier molecular orbitals (HOMO and LUMO) involved in the primary electronic transition of Cy-(Indo)$_2$, illustrating the non-bonding character of the HOMO and the π*-antibonding nature of the LUMO. (c) Energy level diagram showing the ground state, first singlet excited state, and first triplet excited state of Cy-(Indo)$_2$. (d) and (e) Time dependent UV-vis spectra of Cy-(Indo)$_2$ along with DPBF after irradiation with white light for 11 min and a 740 nm LED for 20 min, respectively. (f) Time dependent fluorescence spectra of Cy-(Indo)$_2$ along with H2DCFDA after irradiation under a 740 nm LED for 1 min.

© 2026 The Author(s). Published by the Royal Society of Chemistry

Open Access Article. Published on 13 January 2026. Downloaded on 4/16/2026 7:27:41 PM. This article is licensed under a Creative Commons Attribution-NonCommercial 3.0 Unported Licence.

by a calculated oscillator strength of 1.67, indicative of a significant transition probability and supporting the potential for photoactivation even at longer wavelengths.

As our MD simulations confirmed the formation of stable dimer and trimer aggregates of Cy-$(Indo)_2$, we performed HOMO and LUMO calculations on a representative dimer structure extracted from the MD trajectory. The computed frontier orbitals of the dimer revealed that both the HOMO and LUMO were predominantly localized in the central regions of the monomer units, with minimal contribution from the chlorine-substituted periphery (Fig. S18). The spatial distribution indicated that the key electronic interactions were confined within the conjugated cores of the monomers, even in the aggregated state. Moreover, the orbital diagrams in Fig. 3b were based on natural transition orbitals (NTOs), which were excited state descriptors that visualized the most probable electronic transitions. These NTOs offered complementary insights into the photophysical behaviour of the system by identifying the regions of the molecule involved in the excitation process.

Beyond the ground-state electronic structure, the excited-state energy landscape was also examined to assess the photophysical suitability of Cy-$(Indo)_2$ for photodynamic therapy. As depicted in Fig. 3c, the energy separation between the S_0 and the first singlet excited state (S_1) is calculated to be 2.37 eV, while the singlet–triplet energy gap (ΔE_{ST}) is 1.09 eV. The spin–orbit coupling (SOC) between the S_1 and T_1 states was determined to be 0.066 cm^{-1}, a value sufficient to promote intersystem crossing (ISC) and facilitate efficient population of the T_1 state. Given the stabilization of the T_1 state, the triplet-state lifetime was also evaluated and found to be 40.6 μs—a duration adequate for energy transfer to molecular oxygen, enabling singlet oxygen generation ($^1O_2$). Collectively, these results highlighted the photophysical suitability of Cy-$(Indo)_2$ as a photosensitizer, even under conditions of relatively weak absorption at 730–740 nm.

Hence, to evaluate the phototherapy effect, we irradiated Cy-$(Indo)_2$ under 740 nm LED light (0.9 W cm^{-2}). Unfortunately, we failed to observe any heat generation from Cy-$(Indo)_2$ to use it for photothermal therapy (PTT). Furthermore, to evaluate the photodynamic effect, we irradiated Cy-$(Indo)_2$ at 4 μM concentration in DMSO under white light as well as under a 740 nm LED (0.9 W cm^{-2}) to assess the generation of reactive oxygen species (ROS) by 1,3-diphenylisobenzofuran (DPBF), which showed λ_{max} = 417 nm. In the presence of ROS, DPBF should be converted into 1,2-dibenzoylbenzene (DBB) to reduce the absorbance peak of 417 nm. In the UV-vis spectra, we visualized that, under white light and a 740 nm LED, Cy-$(Indo)_2$ reduced the intensity of the peak at 417 nm dramatically within 11 and 20 min, respectively, in the presence of DPBF (Fig. 3d and e). We further assessed the generation of singlet oxygen species ($^1O_2$) by 9,10-anthracenediyl-bis (methylene) dimalonic acid (ABDA) by monitoring the absorbance of ABDA at 400 nm by UV-vis spectroscopy. We incubated Cy-$(Indo)_2$ with ABDA in water and irradiated it under a 740 nm LED (0.9 W cm^{-2}) for 10 min. The reduction in absorbance at 400 nm in the UV-vis spectra confirmed that under 740 nm LED irradiation, Cy-$(Indo)_2$ generated $^1O_2$ (Fig. S19a).

We also evaluated the generation of ROS by an H2DCFDA assay, which produces a green fluorescence signal at λ_{em} = 525 nm after reacting with the ROS. We incubated Cy-$(Indo)_2$ with H2DCFDA and irradiated it under a 740 nm LED (0.9 W cm^{-2}) in a time-dependent manner, followed by fluorescence emission spectroscopy. We found that Cy-$(Indo)_2$ increased the fluorescence emission of the reaction mixture at λ_{em} = 525 nm remarkably within 60 seconds under 740 nm LED irradiation (Fig. 3f). To further check if Cy-$(Indo)_2$ can generate ROS under NIR-II light, we incubated Cy-$(Indo)_2$ with DPBF and irradiated it under a 940 nm LED followed by monitoring the absorbance at 417 nm by UV-vis spectroscopy. Unfortunately, no generation of ROS was observed even after 10 min (Fig. S19b). This observation was expected as Cy-$(Indo)_2$ did not show any significant absorbance after 800 nm in the UV-vis spectra. These DPBF and H2DCFDA assays confirmed the generation of ROS through the photodynamic effect from Cy-$(Indo)_2$ under 740 nm light irradiation.

Moreover, to estimate the photostability, we irradiated Cy-$(Indo)_2$ in DMSO and water under a 740 nm LED (0.9 W cm^{-2}) for 10 min and monitored the absorbance at 650 nm by UV-vis spectroscopy. It was observed that Cy-$(Indo)_2$ showed no change in absorbance in DMSO even after 10 min of 740 nm LED irradiation (Fig. S20a). However, in water, a gradual decrease in absorbance at 650 nm was observed for 10 min irradiation (Fig. S20b). This time dependent photo-irradiation confirmed that Cy-$(Indo)_2$ is highly photostable in DMSO, but a little photo-unstable in water after 10 min under 740 nm light irradiation. The lack of prolonged photostability in water could be a potential limitation for Cy-$(Indo)_2$.

We further hypothesized that the cationic pentamethine cyanine moiety would lead to mitochondrial accumulation. To validate our hypothesis, we treated HCT-116 colon cancer cells with Cy-$(Indo)_2$ in a time-dependent manner for 3 h and 6 h followed by mitochondrial staining with MitoTracker Green dye. The live cells were then visualized by confocal microscopy. The confocal images showed that red fluorescent Cy-$(Indo)_2$ successfully localized into the green fluorescent mitochondria to produce merged yellow fluorescent signals within 3 h with a high Pearson's correlation coefficient (PCC) = 0.85 and 0.88 at 3 h and 6 h, respectively (Fig. 4a and b and Fig. S21). Moreover, we also visualized the long, thin, filamentous and elongated morphology of healthy mitochondria stained by Cy-$(Indo)_2$, which indicated that our Cy-$(Indo)_2$ can also be utilized to image mitochondria in cancer cells. We further visualized the localization of Cy-$(Indo)_2$ into the endoplasmic reticulum (ER) as mitochondria and the ER share a common membrane. We treated HCT-116 cells with Cy-$(Indo)_2$ for 3 h and 6 h and stained the ER with ER-Tracker Green dye followed by visualization of the live cells under confocal microscopy. The confocal images exhibited that Cy-$(Indo)_2$ marginally homed into the ER with much lower PCC = 0.65 and 0.68 at 3 h and 6 h, respectively (Fig. 4c and Fig. S22a). Moreover, we can clearly visualize that in most of the cells, red fluorescent Cy-$(Indo)_2$ and green fluorescent ER did not overlap. We further visualized the homing of Cy-$(Indo)_2$ into other organelles like the Golgi apparatus and lysosomes. We treated HCT-116 cells with

 © 2026 The Author(s). Published by the Royal Society of Chemistry

Open Access Article. Published on 13 January 2026. Downloaded on 4/16/2026 7:27:41 PM.
This article is licensed under a Creative Commons Attribution-NonCommercial 3.0 Unported Licence.

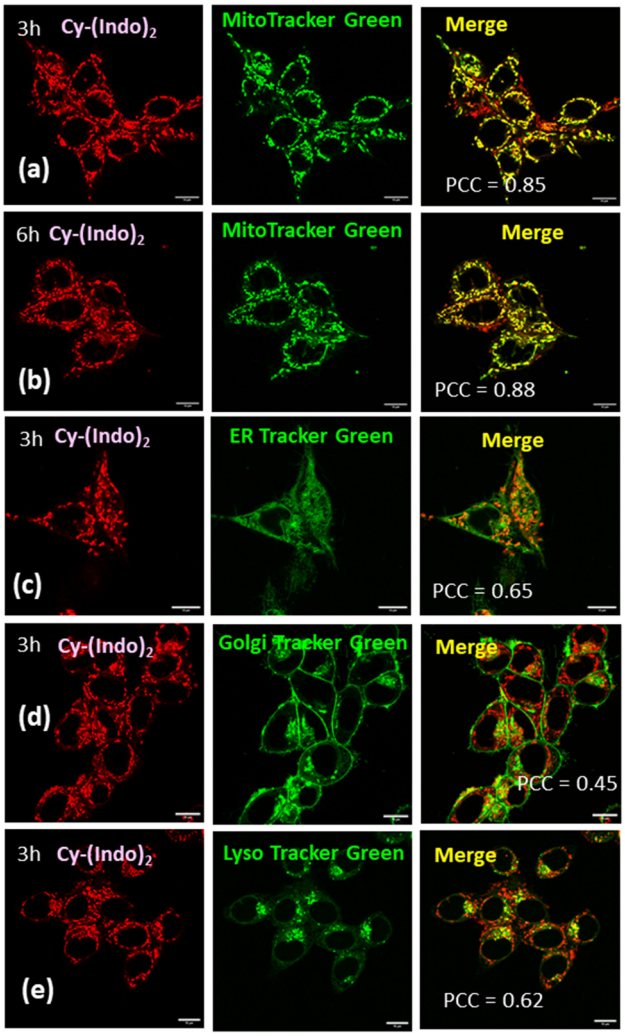

Fig. 4 Confocal laser scanning microscopy images of HCT-116 cells incubated with Cy-$(Indo)_2$ for 3 h and 6 h, respectively. (a) and (b) Mitochondria were stained with MitoTracker Green dye. (c) The ER was stained by ER-Tracker Green dye. (d) and (e) The Golgi apparatus and lysosomes were stained by Golgi Tracker Green and LysoTracker Green dyes, respectively. Scale bar = 10 μm.

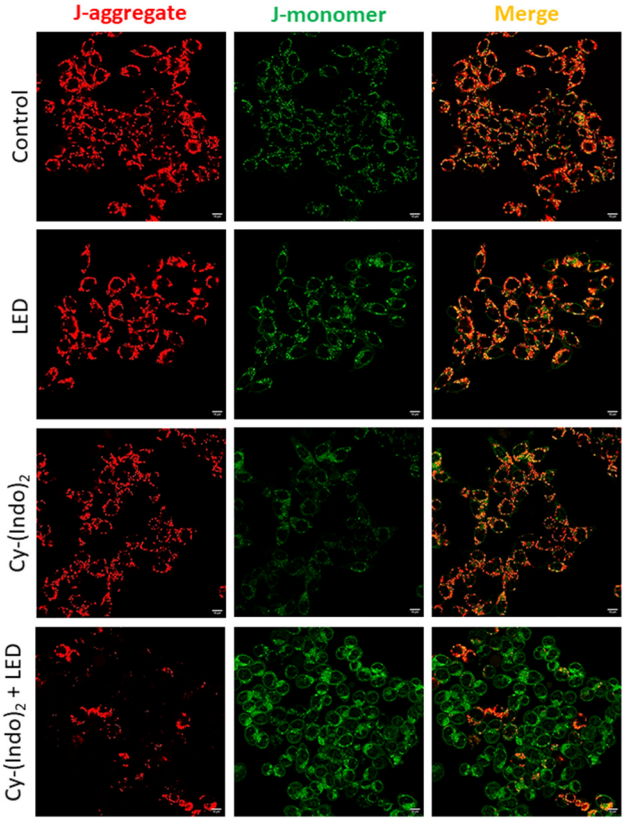

Fig. 5 Confocal laser scanning microscopy images of the HCT-116 cells after incubation with Cy-$(Indo)_2$ for 24 h followed by irradiating with or without a 740 nm LED (0.9 W cm^{-2}) for 10 min. The cells were then stained with JC1 dye. Red and green signals indicate J-aggregates and J-monomers, respectively. Scale bar = 10 μm.

Cy-$(Indo)_2$ for 3 h followed by staining the Golgi apparatus and lysosomes with Golgi Tracker Green and LysoTracker Green dyes, respectively, and visualized them under confocal microscopy. The confocal images showed that Cy-$(Indo)_2$ homed inconsequentially into the Golgi apparatus and lysosomes with very low PCC = 0.45 and 0.62, respectively (Fig. 4d and e and Fig. S22b and c). The organelle homing efficiency from the PCC calculations (Fig. S22d) clearly confirmed that Cy-$(Indo)_2$ homed successfully into the mitochondria selectively within 3 h compared to the other organelles.

After localizing into mitochondria, we evaluated the effect of Cy-$(Indo)_2$ on mitochondrial outer membrane permeabilization (MOMP) under light irradiation. We treated HCT-116 cells with Cy-$(Indo)_2$ for 24 h followed by irradiation under a 740 nm LED (0.9 W cm^{-2}) for 10 min. We then stained the cells with JC1 dye, which emits red fluorescence signals (590 nm) when aggregated inside healthy mitochondria and emits a green fluorescence signal (525 nm) when in monomeric form in the cytosol after mitochondrial membrane depolarization. As a control, we also treated the HCT-116 cells with (a) Cy-$(Indo)_2$ for 24 h without light irradiation, (b) with only 740 nm LED (0.9 W cm^{-2}) irradiation for 10 min and (c) without Cy-$(Indo)_2$ and light irradiation. From the confocal images (Fig. 5), it was observed that non-treated control cells, only LED-treated cells and only Cy-$(Indo)_2$-treated cells all showed high intensity red and green fluorescence signals with green/red = 0.2, which confirmed the presence of healthy non-polarized mitochondria. However, when the HCT-116 cells were treated with Cy-$(Indo)_2$ under light irradiation, the green fluorescence signal intensity increased remarkably compared to the red fluorescence signal intensity with green/red = 23.8 (Fig. 5 and Fig. S23a and b).

To further visualize the mitochondrial morphology damage, we treated HCT-116 cells with Cy-$(Indo)_2$ for 24 h and irradiated the cells with a 740 nm (0.9 W cm^{-2}) LED for 10 min, followed by staining the mitochondria with MitoTracker Green dye and the cells were visualized under confocal microscopy. From the confocal images, it was observed that non-treated control cells and the cells treated with only 740 nm light (0.9 W cm^{-2}) for 10 min exhibited a fine, filamentous and elongated mitochondrial morphology, indicating healthy undamaged mitochondria

Open Access Article. Published on 13 January 2026. Downloaded on 4/16/2026 7:27:41 PM.
This article is licensed under a Creative Commons Attribution-NonCommercial 3.0 Unported Licence.

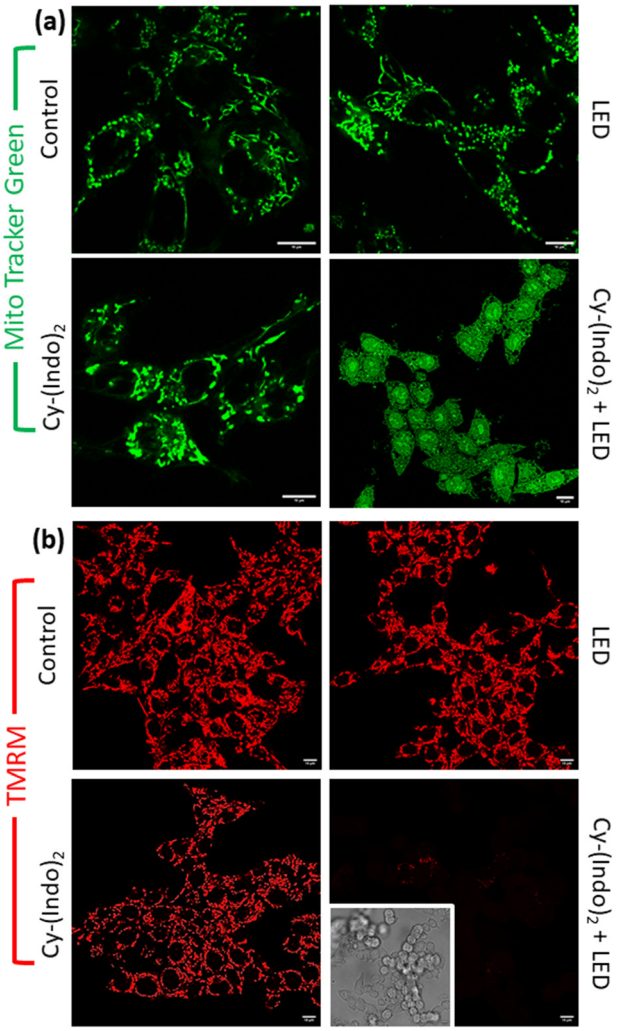

Fig. 6 Confocal laser scanning microscopy images of the HCT-116 cells after treatment with Cy-$(Indo)_2$ for 24 h followed by irradiating with or without a 740 nm LED for 10 min. The cells were stained with (a) MitoTracker Green dye and (b) TMRM (red) dye. Scale bar = 10 μm.

(Fig. 6a and Fig. S24a). On the other hand, the cells treated with only Cy-$(Indo)_2$ without any light irradiation showed a mixture of elongated healthy mitochondria along with punctate damaged structures, which indicated partial mitochondrial damage. In contrast, the treatment of the cells with Cy-$(Indo)_2$ under 740 nm (0.9 W cm^{-2}) light irradiation completely abolished any trace of elongated and filamentous mitochondrial morphology, keeping only the green fluorescent punctate structure, confirming mitochondrial morphological damage.

To confirm the mitochondrial damage, we treated HCT-116 cells with Cy-$(Indo)_2$ for 24 h and irradiated them under a 740 nm (0.9 W cm^{-2}) LED light for 10 min followed by staining the healthy mitochondria by positively charged red fluorescent TMRM dye. When mitochondria are damaged, TMRM would be effluxed from the cells. The cells were then visualized under confocal microscopy, which exhibited that the cells without any treatment and treated with only 740 nm light for 10 min showed high red fluorescence intensity with typical elongated and filamentous mitochondrial morphology, confirming undamaged healthy mitochondria (Fig. 6b and Fig. S24b). On the other hand, only Cy-$(Indo)_2$ treated cells showed reduced (1.5 fold) red fluorescence signal intensity with elongated mitochondrial morphology representing partial mitochondrial damage. However, the HCT-116 cells treated with Cy-$(Indo)_2$ under 740 nm light showed a remarkable decrease in the red fluorescence intensity (17 fold) compared to the control cells and only light treated cells (Fig. 6b and Fig. S24b and c). These JC1, mito-morphology visualization and TMRM assay unequivocally confirm the impairment of mitochondrial outer membrane permeabilization (MOMP) by Cy-$(Indo)_2$ under the irradiation of 740 nm light.

We hypothesized that Cy-$(Indo)_2$ will generate reactive oxygen species (ROS) under light irradiation through a photodynamic effect. Moreover, the impairment of mitochondria by Cy-$(Indo)_2$ under light irradiation would also lead to sub-cellular ROS. To assess the generation of sub-cellular ROS, we treated HCT-116 cells with Cy-$(Indo)_2$ for 24 h and irradiated under 740 nm (0.9 W cm^{-2}) for 10 min. The cells were then incubated with H2DCFDA, which is non-fluorescent, although after reaction with ROS generates green fluorescent DCF dye that can be visualized through confocal microscopy. The confocal images revealed that non-treated control cells as well as only 740 nm LED (0.9 W cm^{-2}) irradiated cells for 10 min showed negligible green fluorescence signals indicating marginal generation of ROS (Fig. 7a and Fig. S25a). On the other hand, Cy-$(Indo)_2$ treated cells (24 h incubation) without any light irradiation showed increased (2.5 fold) green fluorescence signal intensity compared to the control cells as well as the only light irradiated cells, indicating the generation of a small amount of ROS. However, the Cy-$(Indo)_2$ treated cells along with 740 nm light irradiation for 10 min exhibited a remarkable increase (5.3 fold) in green fluorescence intensity compared to the control cells, confirming the excessive generation of ROS (Fig. 7a and Fig. S25b).

Furthermore, we also evaluated the generation of superoxide species because of mitochondrial damage by MitoSox dye, which only shows red fluorescence signals in the presence of superoxide species. We treated HCT-116 cells with Cy-$(Indo)_2$ for 24 h followed by irradiation under 740 nm (0.9 W cm^{-2}) LED light for 10 min. The cells were then treated with MitoSox dye and visualized under confocal microscopy, which demonstrated that non-treated control cells and only 740 nm (0.9 W cm^{-2}) LED treated (10 min) cells hardly showed any red fluorescence signals (Fig. 7b and Fig. S25c), indicating negligible generation of superoxide species. On the other hand, only Cy-$(Indo)_2$ treated cells (24 h incubation) without irradiation under light showed a little increase (3.7 fold) in the red fluorescence signal indicating a very small amount of superoxide species formation. In contrast, cells treated with Cy-$(Indo)_2$ along with irradiation under light exhibited a remarkable increase (7.7 fold) in the red fluorescence intensity, confirming the formation of superoxide species (Fig. S25d). From these H2DCFDA and MitoSox assays, it was evident that Cy-$(Indo)_2$ generated ROS and superoxide species after irradiation under 740 nm light as a result of the photodynamic effect and mitochondrial damage.

© 2026 The Author(s). Published by the Royal Society of Chemistry

Open Access Article. Published on 13 January 2026. Downloaded on 4/16/2026 7:27:41 PM.
This article is licensed under a Creative Commons Attribution-NonCommercial 3.0 Unported Licence.

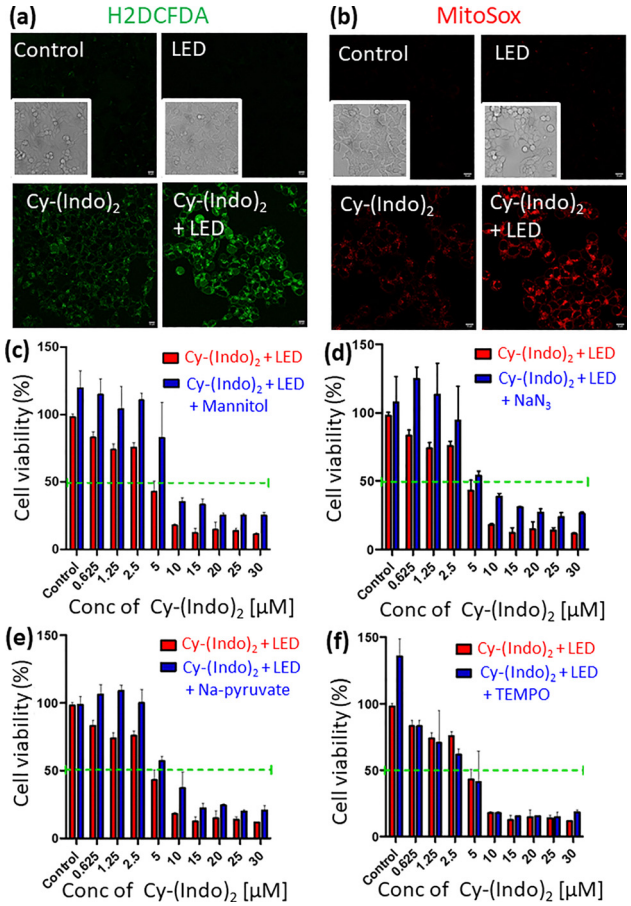

Fig. 7 Confocal laser scanning microscopy of HCT-116 cells treated with Cy-$(Indo)_2$ for 24 h followed by irradiation with/without a 740 nm LED for 10 min. (a) The cells were then incubated with the H2DCFDA dye to visualize ROS generation. (b) Cells were stained with MitoSox (Red) dye to visualize the superoxide generated in the mitochondria. Scale bar = 10 μm. (c)–(f) Viability of HCT-116 cells treated with a combination of Cy-$(Indo)_2$ and mannitol, sodium azide, sodium pyruvate and TEMPO, respectively, for 24 h followed by irradiation under a 740 nm LED (0.9 W cm^{-2}) for 10 min, measured by MTT assay.

To understand the ROS generation through the Type-I or Type-II mechanism, we treated HCT-116 cells with the combination of Cy-$(Indo)_2$ and different ROS quenchers: mannitol (OH radical quencher), sodium azide ($^1O_2$ quencher), TEMPO (superoxide quencher) and sodium pyruvate (H_2O_2 quencher) for 24 h. The cells were then irradiated with a 740 nm LED (0.9 W cm^{-2}) for 10 min and the cell viability was assessed. The MTT assay revealed that mannitol, NaN_3 and *N*-pyruvate decreased the HCT-116 cell death significantly with IC_{50} = 8.3, 5.4 and 5.7 μM, respectively (Fig. 7c–e). In contrast, TEMPO had a marginal effect on HCT-116 cell killing with IC_{50} = 4 μM (Fig. 7f). These MTT assays clearly confirmed that Cy-$(Indo)_2$ under 740 nm light irradiation generated OH radicals, $^1O_2$ and H_2O_2 as ROS leading to a combination of a Type-I and Type-II photodynamic mechanism.

Mitochondrial damage and ROS generation would lead to programmed cell death (apoptosis). To evaluate apoptosis, we treated HCT-116 cells with Cy-$(Indo)_2$ for 24 h followed by irradiation under a 740 nm (0.9 W cm^{-2}) LED for 10 min. The cells were then incubated with FITC-annexin V (green fluorescence) and propidium iodide (PI, red fluorescence) and the cells were sorted through flow cytometry to assess cells in the apoptotic and necrotic stages. The non-treated control cells and only 740 nm (0.9 W cm^{-2}) LED treated (10 min) cells showed 95–96% healthy cells with a marginal number of cells in apoptotic or necrotic stages (Fig. 8a). On the other hand, only Cy-$(Indo)_2$ treated cells showed 11.2% cells in the early apoptotic stage. However, from the flow cytometry analysis, it was measured that Cy-$(Indo)_2$ treatment in combination with light irradiation induced a remarkable increase in the early (54.7%) and late apoptosis (37.3%) cell population.

To further visualize apoptosis, we treated HCT-116 cells with Cy-$(Indo)_2$ for 24 h followed by irradiation under 740 nm (0.9 W cm^{-2}) for 10 min. The cells were then stained with FITC-annexin V (green) and propidium iodide (PI, red)

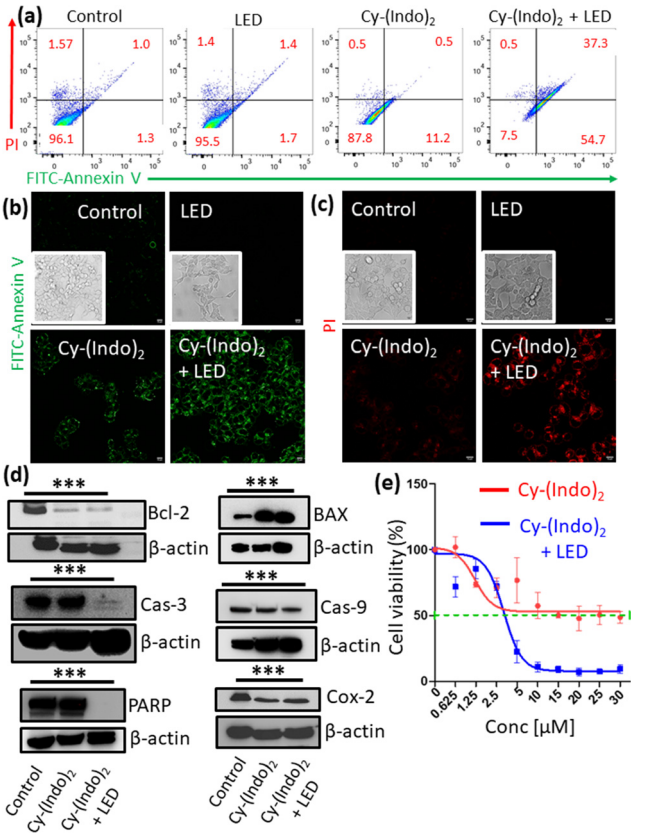

Fig. 8 (a) Flow cytometry analysis of HCT-116 cells after treatment with Cy-$(Indo)_2$ for 24 h followed by irradiation with/without 740 nm LED for 10 min to observe apoptosis. (b) and (c) Confocal laser scanning microscopy images of the HCT-116 cells after treatment with Cy-$(Indo)_2$ for 24 h followed by irradiating with or without a 740 nm LED for 10 min. The cells were then stained with FITC-annexin V (green) and PI (red), respectively. Scale bar = 10 μm. (d) Western blot images of Bcl-2, BAX, Cas-3, Cas-9, PARP and Cox-2 in HCT-116 cells after treatment with Cy-$(Indo)_2$ for 24 h followed by irradiation with or without a 740 nm LED for 10 min. *** $p < 0.0001$, the p value is calculated using two-way ANOVA. (e) Viability of the HCT-116 cells after dose dependent treatment with Cy-$(Indo)_2$ for 24 h followed by irradiating them with or without a 740 nm LED.

© 2026 The Author(s). Published by the Royal Society of Chemistry

Open Access Article. Published on 13 January 2026. Downloaded on 4/16/2026 7:27:41 PM. This article is licensed under a Creative Commons Attribution-NonCommercial 3.0 Unported Licence.

separately and observed under confocal microscopy to assess early/late apoptosis and late apoptosis/necrosis, respectively. From the confocal images (Fig. 8b and Fig. S26a), it was observed that non-treated control cells as well as cells treated with only 740 nm light for 10 min hardly produced any green fluorescence signals, indicating no induction of early/late apoptosis. On the other hand, only Cy-$(Indo)_2$ treated cells (24 h incubation) showed little increase (5.4 fold) in green fluorescence signals suggesting marginal induction of early/late apoptosis. However, the cells treated with Cy-$(Indo)_2$ under light irradiation exhibited a remarkable increase (12.4 fold) in the green fluorescence signals compared to the control cells confirming the induction of early/late apoptosis (Fig. S26b). Similarly, Fig. 8c showed that control cells, only light treated cells and only Cy-$(Indo)_2$ treated cells hardly exhibited any red fluorescence signals, indicating negligible late apoptosis/necrosis induction. In contrast, Cy-$(Indo)_2$ treated cells along with light irradiation exhibited remarkably increased intensity of the red fluorescence signals (12.1 fold) (Fig. S26c and d), confirming the induction of late apoptosis/necrosis.

We also evaluated the induction of apoptosis by measuring the expression of anti-apoptotic Bcl-2, caspase-3, caspase-9 and PARP, as well as pro-apoptotic BAX proteins in cells by gel electrophoresis. We treated HCT-116 cells with Cy-$(Indo)_2$ for 24 h followed by irradiation at 740 nm (0.9 W cm^{-2}) for 10 min. The cellular proteins were harvested, and gel electrophoresis was performed. From the western blot analysis, we observed that Cy-$(Indo)_2$ without any light irradiation reduced the expression of anti-apoptotic Bcl-2 by 3.2 fold compared to the non-treated control cells. On the other hand, Cy-$(Indo)_2$ treatment along with light irradiation reduced the expression of Bcl-2 by 3.9 fold (Fig. 8d and Fig. S27a). Interestingly, under light irradiation, Cy-$(Indo)_2$ remarkably reduced the expression of Cas-3, PARP and Cas-9 by 9.3, 13.3 and 4.7-fold, respectively, compared to the non-treated control cells (Fig. 8d and Fig. S28 and S29a). On the other hand, Cy-$(Indo)_2$ increased the expression of pro-apoptotic BAX under light irradiation by 5.5-fold compared to the control cells (Fig. 8d and Fig. S27b). However, Cy-$(Indo)_2$ without any light irradiation hardly reduced the expression of Cas-3, PARP and Cas-9, which indicated the phototherapy effect of Cy-$(Indo)_2$.

As one of the targets of indomethacin V is Cox-2 protein, we also evaluated the expression of Cox-2 in HCT-116 cells by gel electrophoresis. The western blot analysis also revealed that Cy-$(Indo)_2$ without and under light irradiation reduced the expression of Cox-2 by 1.7 fold and 1.8 fold compared to the non-treated control cells (Fig. 8d and Fig. S29b). It was reported that proteolytic cleavage of Cox-2 happens in HCT-116 cells where the cleaved protein fraction is responsible for the proliferation of cancer cells.[49,50] Interestingly, herein, we observed a decrease in the cleaved Cox-2, which was shown to be decreased by the treatment of NSAIDs like ibuprofen and aspirin. Both the confocal microscopy and gel electrophoresis confirmed that Cy-$(Indo)_2$ induced apoptosis in the presence of 740 nm light irradiation by reducing the expression of Bcl-2, Cas-3, PARP and Cox-2.

Induction of apoptosis would lead to cancer cell death. To evaluate colon cancer cell death, we treated HCT-116 cells with Cy-$(Indo)_2$ in a dose-dependent manner for 24 h followed by irradiation under 740 nm (0.9 W cm^{-2}) for 10 min and measured the cell viability by MTT assay. From the cell viability assay, it was observed that Cy-$(Indo)_2$ induced outstanding cell death under light irradiation with IC_{50} = 3.6 μM compared to Cy-$(Indo)_2$ without any light irradiation, having IC_{50} = 15 μM (Fig. 8e). We also treated HeLa cervical cancer cells with Cy-$(Indo)_2$ in a dose-dependent manner for 24 h followed by irradiation under 740 nm (0.9 W cm^{-2}) for 10 min and performed an MTT assay. In HeLa cells, Cy-$(Indo)_2$ induced a cell killing effect with IC_{50} = 2.5 μM under light irradiation compared to IC_{50} = 24.8 μM for Cy-$(Indo)_2$ without any light irradiation (Fig. S30a). To ensure that pentamethine cyanine dicarboxylic acid (**9**, Fig. S30b, S31 and S32) has no effect in inducing cancer cell death under light irradiation, we further treated HCT-116 cells with compound **9** in a dose-dependent manner for 24 h followed by irradiation with 740 nm (0.9 W cm^{-2}) for 10 min and an MTT assay was performed. The MTT assay clearly exhibited that compound **9** showed negligible cell killing in the presence as well as in the absence of light irradiation (Fig. S30c), which confirmed the unique photodynamic effect of Cy-$(Indo)_2$ under 740 nm light irradiation in HCT-116 and HeLa cells. We further evaluated the effect of Cy-$(Indo)_2$ in non-cancerous Cos-7 kidney cells by incubating with Cy-$(Indo)_2$ in a dose-dependent manner for 24 h followed by irradiation under 740 nm (0.9 W cm^{-2}) for 10 min. The MTT assay revealed that Cy-$(Indo)_2$ induced much less cytotoxicity in Cos-7 cells with IC_{50} = 17.5 μM under light irradiation, whereas Cy-$(Indo)_2$ showed much less cell killing without light irradiation having IC_{50} = 28.8 μM (Fig. S30d). To understand the difference in cell killing effect in cancer cells and non-cancerous cells, we evaluated the cellular uptake of Cy-$(Indo)_2$ in HCT-116 cells and Cos-7 cells in a time-dependent manner. We treated HCT-116 and Cos-7 cells with Cy-$(Indo)_2$ for 6 h, 12 h and 24 h followed by visualizing the cells under confocal microscopy. To our surprise, we observed that the red fluorescence intensity gradually increased for Cy-$(Indo)_2$ treated cells from 6 h to 12 h to 24 h indicating temporal homing of Cy-$(Indo)_2$ into the HCT-116 cells (Fig. S33a). However, in the Cos-7 cells, we observed very weak red fluorescence intensity of Cy-$(Indo)_2$ even at the 24 h time point, indicating much lower cellular uptake of Cy-$(Indo)_2$ into the Cos-7 cells (Fig. S33b). We anticipated the improved uptake of Cy-$(Indo)_2$ in HCT-116 cells compared to Cos-7 cells due to the higher expression of the Cox-2 enzyme in HCT-116 related to Cos-7 cells.[51,52] Furthermore, we also incubated HCT-116 cells with compound **9** at 6 h, 12 h and 24 h time points followed by visualization of the cells under confocal microscopy. We observed a very weak red fluorescence signal in HCT-116 cells confirming negligible uptake of compound **9** in HCT-116 cells even after 24 h (Fig. S33c). This cellular uptake experiment evidently confirmed that Cy-$(Indo)_2$ efficiently homed into HCT-116 cells compared to Cos-7 cells. Furthermore, compound **9** was also not taken up by HCT-116 cells compared to Cy-$(Indo)_2$. These

© 2026 The Author(s). Published by the Royal Society of Chemistry

Open Access Article. Published on 13 January 2026. Downloaded on 4/16/2026 7:27:41 PM. This article is licensed under a Creative Commons Attribution-NonCommercial 3.0 Unported Licence.

uptake studies explained the difference in cell killing ability of Cy-$(Indo)_2$ and compound **9** in cancer cells as well as non-cancerous cells. However, *in vivo* animal experiments need to be performed to explore the feasibility of Cy-$(Indo)_2$ to be translated into the clinic for cancer chemo-photodynamic therapy.

Conclusions

In conclusion, herein, we have designed, and synthesized a mitochondria targeted small molecule [Cy-$(Indo)_2$] photodynamic probe consisting of pentamethine cyanine as a donor–π–acceptor for simultaneous mitochondria targeting, fluorescent imaging and photodynamic therapy, as well as indomethacin V as a drug to target Cox-2 in mitochondria through a concise synthetic strategy. This Cy-$(Indo)_2$ self-assembled into nanoscale spherical particles having 284 nm diameter and high positive surface charge, and generated reactive oxygen species (ROS) under 740 nm LED irradiation within 20 min. MD simulations and TD-DFT were performed to confirm the self-assembly of Cy-$(Indo)_2$ into nanoparticles as well as to demonstrate enough spin–orbit coupling to stabilize and increase the lifetime of T1 for efficient PDT. Cy-$(Indo)_2$ homed efficiently into the mitochondria of HCT-116 colon cancer cells within 3 h. Upon irradiation under 740 nm LED light, Cy-$(Indo)_2$ impaired mitochondria through mitochondrial outer membrane permeabilization (MOMP) followed by mitochondrial morphology damage, leading to the generation of ROS and reactive superoxide species to trigger apoptosis through anti-apoptotic Bcl-2, Cas-3, PARP, Cas-9 and Cox-2 inhibition towards remarkable HCT-116 cell killing without showing any toxicity to the non-cancerous Cos-7 cells. The lack of prolonged photostability in water as well as absorbance in the lower NIR region (650 nm) could be potential limitations of Cy-$(Indo)_2$. However, this novel Cy-$(Indo)_2$ showed potential in mitochondria targeted photodynamic therapy towards next generation non-invasive cancer therapy.

Conflicts of interest

There are no conflicts to declare.

Data availability

The data supporting this article have been included as part of the supplementary information (SI). Supplementary information contains materials, methods, $^{1}H/^{13}C$ NMR spectra, HR-MS spectra, DLS, SEM, AFM and confocal images. See DOI: https://doi.org/10.1039/d5ma00853k.

Acknowledgements

SB acknowledges IIT Gandhinagar, Gujarat Council on Science and Technology (GUJCOST/STI/R&D/2020-21/1302) and Science and Engineering Research Board (CRG/2020/001127) for funding. TM thanks IIT Gandhinagar for the doctoral fellowship. PK and Sanyam acknowledge CSIR-UGC-JRF for the doctoral fellowship. Sanyam and AM thank PARAM Ananta for computational resources.

References

1 A. Trifunovic, A. Wredenberg, M. Falkenberg, J. N. Spelbrink, A. T. Rovio, C. E. Bruder, M. Bohlooly, S. Gidlöf, A. Oldfors, R. Wibom, J. Törnell, H. T. Jacob and N. Larsson, *Nature*, 2004, **429**, 417.
2 R. A. J. Smith, R. C. Hartley, H. M. Cochemé and M. P. Murphy, *Trends Pharmacol. Sci.*, 2012, **33**, 341.
3 P. S. Ward and C. B. Thompson, *Cancer Cell*, 2012, **21**, 297.
4 N. S. Chandel, *BMC Biol.*, 2014, **12**, 34.
5 L. Galluzzi, K. Oliver and K. Guido, *Nat. Rev. Mol. Cell Biol.*, 2012, **13**, 780.
6 S. E. Calvo and V. K. Mootha, *Annu. Rev. Genomics Hum. Genet.*, 2010, **11**, 25.
7 J. Nunnari and A. Suomalainen, *Cell*, 2012, **148**, 1145.
8 V. Gogvadze, S. Orrenius and B. Zhivotovsky, *Trends Cell Biol.*, 2008, **18**, 165.
9 L. K. Boroughs and R. J. DeBerardinis, *Nat. Cell Biol.*, 2015, **17**, 351.
10 S. Patil, D. Ghosh, M. Radhakrishna and S. Basu, *ACS Med. Chem. Lett.*, 2020, **11**, 23.
11 A. Bajpai, Deepshikha, D. Chhabria, T. Mishra, S. Kirubakaran and S. Basu, *Bioorg. Med. Chem.*, 2022, **64**, 116759.
12 S. Pustylnikov, F. Costabile, S. Beghi and A. Facciabene, *Transl. Res.*, 2018, **202**, 35.
13 G. Battogtokh, Y. Y. Cho, J. Y. Lee, H. S. Lee and H. C. Kang, *Acta Pharm. Sin. B*, 2018, **8**, 862–880.
14 S. Luo, X. Dang, J. Wang, C. Yuan, Y. Hu, S. Lei, Y. Zhang, D. Lu, F. Jiang and L. Fu, *Bioorg. Chem.*, 2021, **114**, 105055.
15 A. Bajpai, N. N. Desai, S. Pandey, C. Shukla, B. Datta and S. Basu, *ACS Appl. Bio Mater.*, 2021, **4**, 6799.
16 Y. E. Liu and Y. Shi, *MedComm*, 2020, **1**, 129.
17 M. Škrtić, S. Sriskanthadevan, B. Jhas, M. Gebbia, X. Wang, Z. Wang, R. Hurren, Y. Jitkova, M. Gronda, N. Maclean, C. K. Lai, Y. Eberhard, J. Bartoszko, P. Spagnuolo, A. C. Rutledge, A. Datti, T. Ketela, J. Moffat, B. H. Robinson, J. H. Cameron, J. Wrana, C. J. Eaves, M. D. Minden, J. C. Wang, J. E. Dick, K. Humphries, C. Nislow, G. Giaever and A. D. Schimmer, *Cancer Cell*, 2011, **20**, 674.
18 D. Wang, J. Wang, G. M. C. Bonamy, S. Meeusen, R. G. Brusch, C. Turk, P. Yang and P. G. Schultz, *Angew. Chem. Int. Ed.*, 2012, **51**, 9302.
19 L. Leanza, M. Romio, A. K. Becker, M. Azzolini, L. Trentin, A. Managò, E. Venturini, A. Zaccagnino, A. Mattarei, L. Carraretto, A. Urbani, S. Kadow, L. Biasutto, V. Martini, F. Severin, R. Peruzzo, V. Trimarco, J. H. Egberts, C. Hauser, A. Visentin, G. Semenzato, H. Kalthoff, M. Zoratti, E. Gulbins, C. Paradisi and I. Szabo, *Cancer Cell*, 2017, **31**, 516.

© 2026 The Author(s). Published by the Royal Society of Chemistry

Open Access Article. Published on 13 January 2026. Downloaded on 4/16/2026 7:27:41 PM. This article is licensed under a Creative Commons Attribution-NonCommercial 3.0 Unported Licence.

20 S. Park, K. Baek, I. Shin and I. Shin, *Cell Chem. Biol.*, 2018, **25**, 1242.
21 R. Baskaran, J. Lee and S. G. Yang, *Biomater. Res.*, 2018, **22**, 25.
22 J. Hua, P. Wu, L. Gan, Z. Zhang, J. He, L. Zhong, Y. Zhao and Y. Huang, *Front. Oncol.*, 2021, **11**, 738323.
23 P. Agostinis, K. Berg, K. A. Cengel, T. H. Foster, A. W. Girotti, S. O. Gollnick, S. M. Hahn, M. R. Hamblin, A. Juzeniene, D. Kessel, M. Korbelik, J. Moan, P. Mroz, D. Nowis, J. Piette, B. C. Wilson and J. Golab, *Ca-Cancer J. Clin.*, 2011, **61**, 250.
24 D. E. J. G. J. Dolmans, D. Fukumura and R. K. Jain, *Nat. Rev. Cancer*, 2003, **3**, 380.
25 J. Kou, D. Dou and L. Yang, *Oncotarget*, 2017, **8**, 81591.
26 M. Ethirajan, Y. Chen, P. Joshi and R. K. Pandey, *Chem. Soc. Rev.*, 2011, **40**, 340.
27 J. Tian, B. Huang, M. H. Nawaz and W. Zhang, *Coord. Chem. Rev.*, 2020, **420**, 213410.
28 J. Kou, D. Dou and L. Yang, *Oncotarget*, 2017, **8**, 81591.
29 R. Bonnett, *Chem. Soc. Rev.*, 1995, **24**, 19.
30 P. C. Lo, M. S. Rodríguez-Morgade, R. K. Pandey, D. K. P. Ng, T. Torres and F. Dumoulin, *Chem. Soc. Rev.*, 2020, **49**, 1041.
31 Z. Kejík, J. Hajduch, N. Abramenko, F. Vellieux, K. Veselá, J. Leischner Fialová, K. Petrláková, K. Kučnirová, R. Kaplánek, A. Tatar, M. Skaličková, M. Masařík, P. Babula, P. Dytrych, D. Hoskovec, P. Martásek and M. Jakubek, *Commun. Chem.*, 2024, **7**, 180.
32 J. Yuan, H. Yang, W. Huang, S. Liu, H. Zhang, X. Zhang and X. Peng, *Chem. Soc. Rev.*, 2025, **54**, 341.
33 K. Bilici, S. Cetin, E. Celikbas, H. Y. Acar and S. Kolemen, *Front. Chem.*, 2021, **9**, 707876.
34 J. Zhang, W. Wang, J. Shao, J. Chen and X. Dong, *Coord. Chem. Rev.*, 2024, **516**, 215986.
35 C. J. Zhang, Q. Hu, G. Feng, R. Zhang, Y. Yuan, X. Lu and B. Liu, *Chem. Sci.*, 2015, **6**, 4580.
36 X. Chen, Y. Li, S. Li, M. Gao, L. Ren and B. Z. Tang, *Adv. Funct. Mater.*, 2018, **28**, 1804362.
37 H. W. Liu, X. X. Hu, K. Li, Y. Liu, Q. Rong, L. Zhu, L. Yuan, F. L. Qu, X. B. Zhang and W. Tan, *Chem. Sci.*, 2017, **8**, 7689.
38 W. W. Qin, Z. Y. Pan, D. H. Cai, Y. Li and L. He, *Dalton Trans.*, 2020, **49**, 3562.
39 X. Li, Y. Zhao, T. Zhang and D. Xing, *Adv. Healthcare Mater.*, 2021, **10**, 2001240.
40 B. Guo, M. Wu, Q. Shi, T. J. Dai, S. D. Xu, J. W. Jiang and B. Liu, *Chem. Mater.*, 2020, **32**, 4681.
41 J. Ingle and S. Basu, *ACS Omega*, 2023, **8**, 8925.
42 Y. Matsumura and H. Maeda, *Cancer Res.*, 1986, **46**, 6387–6392.
43 S. George, M. R. Hamblin and H. Abrahamse, *J. Photochem. Photobiol., B*, 2018, **188**, 60–68.
44 T. D. Ridgway and M. D. Lucroy, *Am. J. Vet. Res.*, 2003, **64**, 131–136.
45 Ł. Szymański, M. Ciepielak, A. Cios, M. Palusińska, W. Stankiewicz and S. Lewicki, *Int. J. Mol. Sci.*, 2021, **22**, 11605.
46 W. B. Lim, J. S. Kim, Y. J. Ko, H. I. Kwon, S. W. Kim, H. K. Min, O. Kim, H. R. Choi and O. J. Kim, *Lasers Surg. Med.*, 2011, **43**, 344–352.
47 S. Dani, K. Schütz, E. Dikici, A. Bernhardt and A. Lode, *Sci. Rep.*, 2024, **14**, 9444.
48 J. Ingle, B. Uttam, R. Panigrahi, S. Khatua and S. Basu, *J. Mater. Chem. B*, 2023, **11**, 9732–9741.
49 E. Saadi, R. Sood, I. Dromi, R. Srouji, O. Abu Hatoum, S. Tal and L. Barki-Harrington, *Int. J. Mol. Sci.*, 2020, **21**, 3195.
50 L. H. Hartal-Benishay, S. Tal, A. A. Elkader, O. Ehsainieh, R. Srouji-Eid, T. Lavy, O. Kleifeld, M. Mikl and L. Barki-Harrington, *iScience*, 2024, **27**, 111403.
51 B. Gurram, S. Zhang, M. Li, H. Li, Y. Xie, H. Cui, J. Du, J. Fan, J. Wang and X. Peng, *Anal. Chem.*, 2018, **90**, 5187–5193.
52 B. Wang, J. Fan, X. Wang, H. Zhu, J. Wang, H. Mua and X. Penga, *Chem. Commun.*, 2015, **51**, 792–795.

© 2026 The Author(s). Published by the Royal Society of Chemistry